

# MULTIBAND NONTHERMAL RADIATIVE PROPERTIES OF HESS J1813-178

JUN FANG & LI ZHANG

Department of Physics, Yunnan University, Kunming, China

Draft version June 2, 2010

## ABSTRACT

The source HESS J1813-178 was detected in the survey of the inner Galaxy in TeV  $\gamma$ -rays, and a composite supernova remnant (SNR) G12.8-0.0 was identified in the radio band to be associated with it. The pulsar wind nebula (PWN) embedded in the SNR is powered by an energetic pulsar PSR J1813-1749, which was recently discovered. Whether the TeV  $\gamma$ -rays originate from the SNR shell or the PWN is uncertain now. We investigate theoretically the multiwavelength nonthermal radiation from the composite SNR G12.8-0.0. The emission from the particles accelerated in the SNR shell is calculated based on a semianalytical method to the nonlinear diffusive shock acceleration mechanism. In the model, the magnetic field is self-generated via resonant streaming instability, and the dynamical reaction of the field on the shock is taken into account. Based on a model which couples the dynamical and radiative evolution of a PWN in a non-radiative SNR, the dynamics and the multi-band emission of the PWN are investigated. The particles are injected with a spectrum of a relativistic Maxwellian plus a power law high-energy tail with an index of  $-2.5$ . Our results indicate that the radio emission from the shell can be well reproduced as synchrotron radiation of the electrons accelerated by the SNR shock; with an ISM number density of  $1.4 \text{ cm}^{-3}$  for the remnant, the  $\gamma$ -ray emission from the SNR shell is insignificant, and the observed X-rays and very high energy (VHE)  $\gamma$ -rays from the source are consistent with the emission produced by electrons/positrons injected in the PWN via synchrotron radiation and inverse Compton (IC) scattering, respectively; the resulting  $\gamma$ -ray flux for the shell is comparable to the detected one only with a relatively larger density of about  $2.8 \text{ cm}^{-3}$ . The VHE  $\gamma$ -rays of HESS J1813-178 can be naturally explained to mainly originate from the nebula although the contribution of the SNR shell becomes significant with a denser ambient medium.

*Subject headings:* gamma rays: ISM— ISM: individual objects (HESS J1813-178, G12.8-0.0) - supernova remnants

## 1. INTRODUCTION

The VHE source HESS J1813-178 was discovered with the High Energy Stereoscopic System (HESS) in a survey of the inner Galaxy in VHE  $\gamma$ -rays (Aharonian et al. 2005a). The VHE  $\gamma$ -ray image obtained with the HESS shows a pointlike source with an extension of  $\sim 2.2'$ , and the observed spectrum has a hard photon index  $2.09 \pm 0.08$  (Aharonian et al. 2006). HESS J1813-178 was also detected in VHE  $\gamma$ -rays with the Major Atmospheric Gamma Imaging Cerenkov (MAGIC) telescope. The differential flux given by MAGIC between 0.4 and 10 TeV can be well described by a power law with an index of  $-2.1 \pm 0.2$  (Albert et al. 2006), which is consistent with the result obtained with the HESS.

Firstly, HESS J1813-178 was unidentified, and it was assumed to be a "dark particle accelerator" since no counterpart at lower frequencies was reported ever. However, the shell of the SNR G12.8-0.0 associated with HESS J1813-178 was discovered with a diameter of  $\sim 2.5'$  in a new low-frequency Very Large Array (VLA) 90 cm survey (Brogan et al. 2005). The non-thermal radio flux densities of the shell-type SNR are  $0.65 \pm 0.10$  and  $1.2 \pm 0.08 \text{ Jy}$  at 20 and 90 cm, respectively (Brogan et al. 2005). A highly absorbed X-ray source AX J1813-178, for which the column density is  $10^{23} \text{ cm}^{-2}$ , detected with ASCA is spatially coincident with the SNR. The X-ray emission extending to 10 keV with a sharp cutoff below 2 keV is primarily nonthermal, which can originate either from the SNR shell or from the pulsar wind nebula (PWN) inside the remnant (Brogan et al. 2005). Due to the high column density derived from the ASCA data, a distance of  $\geq 4$

kpc is derived for the source (Brogan et al. 2005).

Moreover, a soft  $\gamma$ -ray source, IGR J18135-1751, was discovered as the counterpart of HESS J1813-178 (Ubertini et al. 2005). It is persistent with a 20–100 keV luminosity of  $5 \times 10^{34} \text{ erg s}^{-1}$  for a distance of 4 kpc. Ubertini et al. (2005) argued that the observed properties of the source in the radio and X-ray bands can be explained with the assumption that the source is a pulsar wind nebula embedded in G12.8-0.0. Furthermore, high-angular resolution X-ray observation with *XMM-Newton* shows that the X-ray emitting object appears as a compact core located in the center of the radio shell-type SNR G12.8-0.0 (Funk et al. 2007). They argued that the source is a composite SNR since the central object shows morphological and spectral resemblance to a PWN.

The observation with *Chandra* on the SNR G12.8-0.0 indicates the X-ray source is a point surrounded by structured diffuse emission that fills the interior of the radio shell (Helfand et al. 2007). The compact source has a spectrum characterized by a power law with an index of  $\sim 1.3$ , typical of young and energetic rotation-powered pulsars, and the morphology of the diffuse emission strongly resembles that of a pulsar wind nebula (Helfand et al. 2007). Recently, an energetic pulsar PSR J1813-1749 with a period of  $\sim 44.7 \text{ ms}$ , a characteristic age of 3.3–7.5 kyr, and a distance of 4.7 kpc by assuming the association with an adjacent young stellar cluster, was discovered in a long, continuous *XMM-Newton* X-ray timing observation (Gotthelf & Halpern 2009). The pulsar was found to be associated with the SNR G12.8-0.0, and it powers the PWN (Gotthelf & Halpern 2009).

High-energy  $\gamma$ -rays can be produced either from SNR shells in which particles are accelerated to relativistic through

the first Fermi process (e.g., Aharonian et al. 2005b, 2007; Berezhko & Völk 2006; Fang & Zhang 2008; Fang et al. 2009; Morlino, Amato & Blasi 2009), or from PWNe powered by the pulsars inside them (e.g., Volpi et al. 2008; Zhang, Chen & Fang 2008; Gelfand, Slane & Zhang 2009). Although the source HESS J1813-178 is pointlike in VHE  $\gamma$ -rays, the possibility of the VHE  $\gamma$ -rays originating from the shell of the remnant cannot be ruled out given the size of the SNR, the angular resolution of the HESS telescope, and the depth of the observations (Albert et al. 2006). In this paper, we study the multiband nonthermal emission from the shell of the SNR G12.8-0.0 and the nebula inside it. The emission from the particles accelerated by the SNR shock is investigated based on a semianalytical method to the nonlinear diffusive shock acceleration mechanism with a free escape boundary proposed by Caprioli et al. (2010b), in which the amplified magnetic field due to resonant streaming instability induced by cosmic rays and the dynamical feedback of this self-generated magnetic field on the shock are taken into account. On the other hand, the dynamics and the multi-band radiative properties of the PWN are investigated basically according to the model in Gelfand, Slane & Zhang (2009), which can self-consistently describe the dynamical and radiative evolution of a pulsar wind nebula in a non-radiative supernova remnant. Recently, based on the long-term two dimensional particle-in-cell simulations, Spitkovsky (2008) found that the particle spectrum downstream of a relativistic shock consists of two components: a relativistic Maxwellian and a power law high-energy tail with an index of  $-2.4 \pm 0.1$ . Different from Gelfand, Slane & Zhang (2009), in which a single power law injection spectrum for the electrons/positrons is employed to discuss the radiative properties during different phase of the PWN, in this paper we argue that the high-energy particles are injected with the spectrum of a relativistic Maxwellian plus a power-law high-energy tail during the evolution, and a kinetic equation is used to obtain the energy distribution of the particles.

## 2. MODEL AND RESULTS

In this section we describe the physics of our model for the particles accelerated by a shock and its multiband nonthermal emission (Section 2.1), the dynamics and multiwavelength radiation of a PWN in the nonradiative shell (Section 2.2), and its implementation to the SNR G12.8-0.0 (Section 2.3).

### 2.1. Particles accelerated by the SNR shock and its emission

The pitch-angle averaged steady-state distribution of the protons accelerated at a shock in one dimension satisfies the diffusive transport equation (Malkov & Drury 2001; Blasi 2002; Amato, Blasi & Gabici 2008),

$$\frac{\partial}{\partial x} \left[ D \frac{\partial}{\partial x} f(x, p) \right] - u \frac{\partial f(x, p)}{\partial x} + \frac{1}{3} \frac{du}{dx} p \frac{\partial f(x, p)}{\partial p} + Q(x, p) = 0, \quad (1)$$

where the coordinate  $x$  is directed along the shock normal from downstream towards upstream,  $D$  is the diffusion coefficient and  $u$  is the fluid velocity in the shock frame, which equals  $u_2$  downstream ( $x > 0$ ) and changes continuously upstream, from  $u_1$  immediately upstream ( $x = 0^-$ ) of the subshock to  $u_0$  at far upstream. For the Bohm diffusion,  $D = pc^2/(3eB)$ , where  $B$  is the local magnetic field strength. The maximum momentum of the protons accelerated by a SNR

increases with time in the free-expansion phase of the SNR due to the efficient magnetic field strength and the constant shock speed. After the beginning of the Sedov-Taylor phase, the maximum momentum drops with time due to the decrease of the shock speed and the efficiency of the magnetic field amplification (Caprioli et al. 2009, 2010a). In this case, particles with higher momentum will escape from the SNR, and this phenomenon can be mimicked by imposing a free escape boundary at a location upstream of the shock, i.e.,  $f(-x_0, p) = 0$  (Caprioli et al. 2010a,b).

With the assumption that the particles are injected at immediate upstream of the subshock, the source function can be written as  $Q(x, p) = Q_0(p)\delta(x)$ . For monoenergetic injection,  $Q_0(p)$  is

$$Q_0(p) = \frac{\eta n_{\text{gas},1} u_1}{4\pi p_{\text{inj}}^2} \delta(p - p_{\text{inj}}), \quad (2)$$

where  $p_{\text{inj}}$  is the injection momentum,  $n_{\text{gas},1}$  is the gas density at  $x = 0^+$  and  $\eta$  is the fraction of particles injected in the acceleration process. With the injection recipe known as thermal leakage,  $\eta$  can be described as  $\eta = 4(R_{\text{sub}} - 1)\xi^3 e^{-\xi^2}/3\pi^{1/2}$  (Blasi, Gabici & Vannoni 2005; Amato, Blasi & Gabici 2008), where  $R_{\text{sub}} = u_1/u_2$  is the compression factor at the subshock and  $\xi$  is a parameter of the order of 2–4 describing the injection momentum of the thermal particles in the downstream region ( $p_{\text{inj}} = \xi p_{\text{th},2}$ ).  $p_{\text{th},2} = (2m_p k_B T_2)^{1/2}$  is the thermal peak momentum of the particles in the downstream fluid with temperature  $T_2$ ,  $m_p$  is the proton mass and  $k_B$  is the Boltzmann constant. The downstream temperature  $T_2$  is calculated with equations (10) and (11) in Caprioli et al. (2009). A relatively large  $\xi = 3.8$ –4.1 is usually employed to investigate the radiative properties of SNRs (e.g., Morlino, Amato & Blasi 2009; Morlino et al. 2009), and we adopt  $\xi = 3.8$  in this paper.

The normalized pressure in cosmic rays is

$$P_c(x) = \frac{4\pi}{3\rho_0 u_0^2} \int_{p_{\text{inj}}}^{\infty} dp p^3 v(p) f(x, p), \quad (3)$$

where  $\rho_0$  is the gas density far upstream of the shock. Magnetic fields can be generated by streaming instability induced by the accelerated particles. With the assumption of the turbulence is generated by the resonant streaming instability, the normalized pressure of the amplified magnetic field can be described as (Caprioli et al. 2009, 2010b)

$$P_w(x) = \frac{v_A}{4u_0} \frac{1 - U^2(x)}{U^{3/2}(x)}, \quad (4)$$

where  $U(x) = u(x)/u_0$ ,  $v_A = B_0/(4\pi\rho_0)^{1/2}$  is the Alfvén velocity,  $B_0$  is the background magnetic field strength. Then the strength of the amplified field is  $\delta B(x) = (8\pi\rho_0 u_0^2 P_w(x))^{1/2}$ , and the magnetic field downstream of the shock is further enhanced by  $B_2 = R_{\text{sub}} B_1$  (Morlino, Amato & Blasi 2009), where  $B_1 = \delta B(0)$  is the amplified magnetic field immediately upstream of the subshock. The effect of turbulent heating is ignored in this paper because the properties of the damping of the magnetic field is still uncertain now, and a new parameter is needed even with the damping phenomenologically taken into account (Caprioli et al. 2010a). Neglecting the effect of turbulent heating, the normalized pressure of the background gas is

$$P_g(x) = \frac{U(x)^{-\gamma}}{\gamma M_0^2}, \quad (5)$$

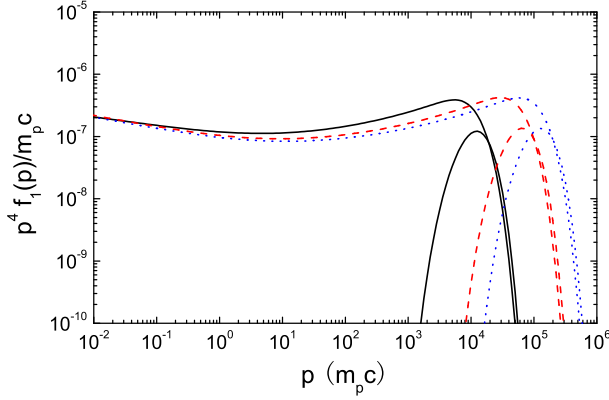


FIG. 1.— Particle spectra at the shock and the escape fluxes ( $p^4 \phi_{\text{esc}}/u_0$ ) with  $\xi = 3.8$ ,  $T_0 = 10^4$  K,  $n_0 = 1.4 \text{ cm}^{-3}$ ,  $B_0 = 5 \mu\text{G}$ ,  $u_0 = 1 \times 10^8 \text{ cm s}^{-1}$ ,  $x_0 = 0.18$  pc (solid line);  $x_0 = 0.9$  pc (dashed line); and  $x_0 = 1.8$  pc (dotted line).

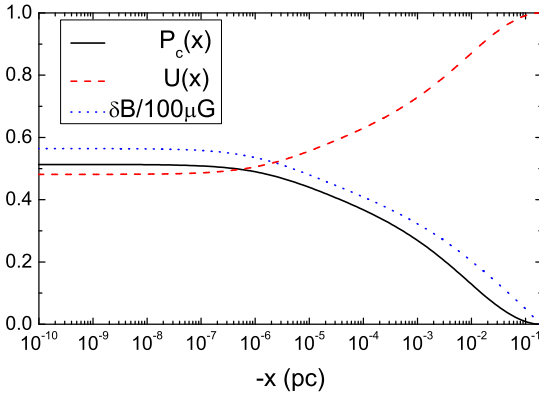


FIG. 2.—  $P_c(x)$  (solid line),  $U(x)$  (dashed line), and  $\delta B/100 \mu\text{G}$  (dotted line) in the upstream region for  $x_0 = 0.9$  pc. Others are the same as Fig. 1.

where  $M_0$  is the sonic Mach number of the shock,  $\gamma = 5/3$  is the adiabatic index. The total compression factor  $R_{\text{tot}}$  is related with the compression factor at the subshock  $R_{\text{sub}}$  through (Caprioli et al. 2009)

$$R_{\text{tot}}^{\gamma+1} = \frac{M_0^2 R_{\text{sub}}^\gamma}{2} \left[ \frac{\gamma+1 - R_{\text{sub}}(\gamma-1)}{1 + \Lambda_B} \right], \quad (6)$$

where

$$\Lambda_B = \frac{P_w(0)}{P_g(0)} [1 + R_{\text{sub}}(2/\gamma - 1)]. \quad (7)$$

Given a value of  $\xi$ , a temperature far upstream of the shock  $T_0$ , a shock velocity  $u_0$ , a background magnetic field  $B_0$ , and  $x_0$ , the particle spectrum at the shock  $f_1(p)$  and the escape flux  $\phi_{\text{esc}}(p) = -[D(x, p) \partial f / \partial x]_{x_0}$  can be obtained with the method proposed in Caprioli et al. (2010b), in which the diffusion coefficient is calculated in the self-generated magnetic field induced by resonant streaming instability of the accelerated particles. In order to show how the protons spectrum is affected by the choice of  $x_0$ , we plot in Fig. 1 the particle spectra at the sub-shock position and the escaping fluxes for three different values of  $x_0$ : 0.18 pc (solid line); 0.9 pc (dashed line); and = 1.8 pc (dotted line). The other parameters are all fixed to:

$\xi = 3.8$ ,  $T_0 = 10^4$  K,  $n_0 = 1.4 \text{ cm}^{-3}$ ,  $B_0 = 5 \mu\text{G}$ ,  $u_0 = 1 \times 10^8 \text{ cm s}^{-1}$ . The particle spectrum for each  $x_0$  is cut off at a maximum momentum  $p_{\text{max}}$ , which increases with the value of  $x_0$ .  $U(x)$ ,  $P_c(x)$  and  $\delta B$  in the upstream region for  $x_0 = 0.9$  pc are indicated in Fig. 2. The amplified magnetic field immediately upstream of the subshock  $B_1$  is  $56 \mu\text{G}$ , which is significantly stronger than the background magnetic field.

The electrons have the same spectrum of the protons up to a maximum energy determined by synchrotron losses. Note that the spectrum of the accelerated electrons at the shock around the cutoff momentum  $p_{\text{max},e}$  is difficult to obtain in a fully nonlinear scenario. With the test particle approximation, the energy spectrum of electrons accelerated by SNR shocks for a strong shock can be described as (Zirakashvili & Aharonian 2007; Blasi 2010)

$$f_e(x, p) = K_{ep} f(x, p) [1 + 0.523(p/p_{\text{max},e})^2] \exp(-p^2/p_{\text{max},e}^2). \quad (8)$$

However, the spectrum cut off by a simple exponential is also employed to reproduce the multiband emission from SNRs (e.g., Fang et al. 2009), and we use this form in this paper, i.e.,

$$f_e(x, p) = K_{ep} f(x, p) \exp(-E(p)/E_{\text{max},e}), \quad (9)$$

where  $E(p)$  is the kinetic energy of the electrons, and the electron/proton ratio  $K_{ep}$  is treated as a parameter. The choice of the cut-off shape of the spectrum has no influence on our results because in this paper we interpret the observed X-ray from emission G12.8-0.0 as due to the PWN inside the remnant. The maximum energy of electrons results equating the synchrotron loss time with the acceleration time. In the context of non linear shock acceleration an approximate solution is given by the following equation (Berezhko et al. 2002)

$$E_{\text{max},e} = 6 \times 10^7 \left( \frac{u_0}{10^8 \text{ cm s}^{-1}} \right) \left[ \frac{R_{\text{tot}} - 1}{R_{\text{tot}}(1 + R_{\text{sub}} R_{\text{tot}})} \left( \frac{10 \mu\text{G}}{B_1} \right) \right]^{1/2} \text{ MeV}, \quad (10)$$

where the magnetic field immediately upstream of the shock,  $B_1$ , is assumed to be compressed by a factor  $R_{\text{sub}}$ .

Assuming the accelerated particles distribute homogeneously and most of the emission is from downstream of the shock, and using the distribution function at the shock to represent the particle distribution in the whole emitting zone, the volume-averaged emissivity for photons produced via p-p interactions can be written as

$$Q(E) = 4\pi n_{\text{gas}} \int dE_p J_p(E_p) \frac{d\sigma(E, E_p)}{dE}, \quad (11)$$

where  $E_p$  is the proton kinetic energy,  $n_{\text{gas}} = R_{\text{tot}} n_0$  is the gas number density downstream of the shock, and  $J_p(E_p) = v p^2 f_0(p) dp / dE_p$  is the volume-averaged proton density and  $v$  is the particles' velocity. We use the differential cross-section for photons  $d\sigma(E, E_p)/dE$  presented in Kamae et al. (2006) to calculate the hadronic  $\gamma$ -rays produced via p-p interaction. Finally, the photon flux observed at the earth can be obtained with

$$F(E) = \frac{V Q(E)}{4\pi d^2}, \quad (12)$$

where  $d$  is the distance from the earth to the source and  $V$  is the average emitting volume of the source. For the accelerated protons, the emitting volume can be estimated by  $V_p \approx (4\pi/3) R_{\text{snr}}^3 / R_{\text{tot}}$  (Ellison et al. 2000), here  $R_{\text{snr}}$  is the radius of the SNR. For the electrons, the thickness of the emitting region can be estimated by solving the

diffusion-convection equation downstream of the shock, i.e.,  $u_2(\partial f_e/\partial x) = D\partial^2/\partial x^2 - f_e/\tau_{\text{syn}}$ , where  $\tau_{\text{syn}}$  is the time scale of the synchrotron radiation (Morlino, Amato & Blasi 2009). The solution shows  $f_e \propto \exp(-x/R_{\text{rim}})$ , and the spatial scale  $R_{\text{rim}}$  is given by (Berezhko & Völk 2004)

$$R_{\text{rim}}(p) = \frac{2D_2/u_2}{\sqrt{1+4D_2/u_2\tau_{\text{syn}}-1}}. \quad (13)$$

As a result of the synchrotron losses, electrons with relatively high energy are confined into a thin rim behind the shock and the total emitting volume is smaller than  $V_p$ . A break in the spectrum occurs for  $p = p_t$ , defined as the momentum where the time scale of the losses equals to the age of the remnant, i.e.  $\tau_{\text{syn}}(p_t) = t_{\text{snr}}$ . In the steady state, the volume of the electrons with higher energies is smaller than that of the protons due to the strong synchrotron losses. Hence  $V_e(p) = V_p$  for  $p \leq p_t$ , while  $V_e(p) = V_p R_{\text{rim}}(p)/(R_{\text{snr}}/3R_{\text{tot}})$  for  $p > p_t$ , where  $p_t$  is determined by  $4\pi R_{\text{snr}}^2 R_{\text{rim}}(p) = V_p$ .

## 2.2. Dynamics and radiative properties of a PWN inside a nonradiative SNR

A PWN is powered by the pulsar which dissipates its rotational energy into the nebula. The spin-down luminosity of a pulsar with a rotation period of  $P$  evolves with time as (e.g., Gaensler & Slane 2006; Slane 2008)

$$\dot{E}(t) = \dot{E}_0 \left(1 + \frac{t}{\tau_0}\right)^{-\frac{n+1}{n-1}}, \quad (14)$$

where  $\tau_0$  is the spin-down time scale of the star,  $\dot{E}_0$  is the initial spin-down power,  $n$  is the braking index of the pulsar, which is equal to 3 for magnetic dipole spin-down.

High-energy particles and magnetic fluxes are injected into the PWN from the terminate shock located where the ram pressure of the unshocked wind is equal to that of the nebula. In this paper, we assume the spin-down power is distributed between electrons and positrons ( $\dot{E}_e(t) = \eta_e \dot{E}(t)$ ), and magnetic fields ( $\dot{E}_B = \eta_B \dot{E}(t)$ ) (e.g., Gelfand, Slane & Zhang 2009). In Gelfand, Slane & Zhang (2009), they used a simple power-law injection spectrum for the electrons/positrons to discuss the radiative properties during different phase of the PWN. However, a broken power-law spectrum is usually needed to reproduce the non-thermal emission of a PWN with multi-band observations (e.g., Atoyan & Aharonian 1996; Venter & de Jager 2006; Slane et al. 2008; Zhang, Chen & Fang 2008). Recently, based on the long-term two-dimensional particle-in-cell simulations, Spitkovsky (2008) found that the particle spectrum downstream of a relativistic shock is a Maxwellian plus a power-law tail with a index of  $2.4 \pm 0.1$ , and this spectrum also was used to investigate the multiband emission from PWNe (e.g., Fang & Zhang 2010; Slane et al. 2010). We assume high-energy particles injected in a PWN are accelerated by the termination shock (TS) which is typically relativistic with a lorentz factor  $\sim 10^6$  with respect to the pulsar wind upstream of the shock. Therefore, we assume the spectrum of the high-energy particles injected in the PWN has the form,

$$Q(E, t) = \begin{cases} C(t) \frac{E}{E_b} \exp\left(-\frac{E}{E_b}\right) & E \leq E_{\min} \\ C(t) \left[ \frac{E}{E_b} \exp\left(-\frac{E}{E_b}\right) + f \left(\frac{E}{E_b}\right)^{-\alpha} \right] & E_{\min} < E \leq E_{\max} \end{cases}, \quad (15)$$

where,  $\alpha = 2.4 \pm 0.1$ ,  $E_b \sim 2.6 \times 10^5 \gamma_{\text{ts},6} \text{ MeV}$ ,  $\gamma_{\text{ts},6}$  is the Lorentz factor of the upstream pulsar wind of the TS in

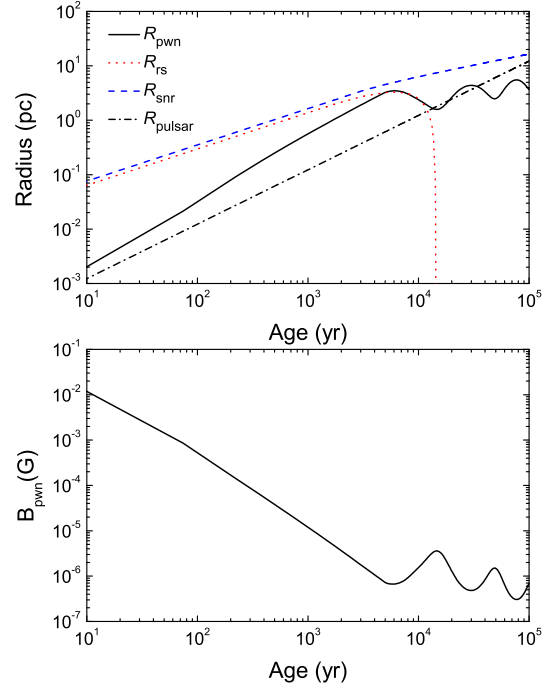


FIG. 3.— Upper panel: radius of the SNR ( $R_{\text{snr}}$ , dashed line), reverse shock ( $R_{\text{rs}}$ , dotted line), PWN ( $R_{\text{pwn}}$ , solid line), and the location of the pulsar ( $R_{\text{pulsar}}$ , dash-dotted line). Lower panel: magnetic field strength in the PWN ( $B_{\text{pwn}}$ ).

units of  $10^6$ ,  $E_{\min} = f_{\min} E_b$  with  $f_{\min} \sim 7$ ,  $f$  is normalized by  $E_{\min}/E_b \exp(-E_{\min}/E_b) = f(E_{\min} E_b)^{-\alpha}$ .  $C(t)$  can be obtained with

$$C(t) = \frac{\dot{E}_e(t)}{2E_b^2 + f \frac{E_b^2}{2-\alpha} \left[ \left(\frac{E_{\max}}{E_b}\right)^{2-\alpha} - \left(\frac{E_{\min}}{E_b}\right)^{2-\alpha} \right]}. \quad (16)$$

Assuming the particles are homogeneously distributed in the PWN, and the energy distribution of these particles in the nebula evolves as

$$\frac{\partial N(E, t)}{\partial t} = \frac{\partial}{\partial E} [\dot{E} N(E, t)] + Q(E, t), \quad (17)$$

where  $\dot{E}$  is the energy-loss rate of the particles with energy  $E$ . Energy-loss mechanisms include synchrotron radiation, IC scattering and adiabatic loss.

The dynamics of the PWN inside the supernova shell is calculated basically following the model presented in Gelfand, Slane & Zhang (2009). The model assumes that the progenitor supernova ejects material with mass  $M_{\text{ej}}$  and energy  $E_{\text{sn}}$  into the ambient matter with a constant density  $\rho_{\text{ISM}}$ . Assuming the PWN has no influence on the dynamics of the forward shock and the reverse shock, the velocity and the radius of the forward shock and the reverse shock of the surrounding SNR are calculated with the equations in Truelove & McKee (1999). The pulsar dissipates energy into the PWN, which sweeps up the supernova ejecta into a thin shell surrounding the nebula, and new particles are injected into the PWN at each time step.

The dynamical evolution of the PWN with the parameters for the SNR G12.8-0.0 (see Table 1) is shown in Fig. 3. The

TABLE 1  
INPUT PARAMETERS FOR THE SNR G12.8-0.0

PARAMETER	VALUE	PARAMETER	VALUE
$d$	4.7 kpc	$E_0^2$	$4.2 \times 10^{38} \text{ erg s}^{-1}$
$E_{\text{sn}}$	$0.4 \times 10^{50} \text{ erg}$	$\tau_{\text{sd}}$	500 yr
$M_{\text{ej}}$	$3M_{\odot}$	$n$	3.0
$n_0$	$1.4 \text{ cm}^{-3}$	$\eta_{\text{B}}$	$1 \times 10^{-4}$
Age	1200 yr	$E_{\text{max}}$	1000 TeV
$T_0$	$10^4 \text{ K}$	$E_{\text{b}}$	$3 \times 10^5 \text{ MeV}$
$B_0$	$5 \mu\text{G}$	$v_{\text{psr}}$	$120 \text{ km s}^{-1}$
$K_{\text{ep}}$	$1.8 \times 10^{-3}$		

radiuses of the SNR ( $R_{\text{snr}}$ ), the reverse shock ( $R_{\text{rs}}$ ), the PWN ( $R_{\text{pwn}}$ ) and the pulsar are indicated by the dashed, dotted, solid and dash-dotted lines, respectively. A velocity of  $120 \text{ km s}^{-1}$  is used in the calculation, which has no influence on the resulting dynamical structure and radiative property of G12.8-0.0 because the young pulsar is safely in the nebula now (see Section 2.3). Initially, the pressure of the PWN is much bigger than the pressure of the surrounding supernova ejecta, so the PWN expands adiabatically into the cold supernova ejecta. The ejecta surrounding the PWN is swept up to a thin shell, which is decelerated by ram pressure since its velocity is bigger than the local sound speed (Gelfand et al. 2007). The mass of the PWN  $M_{\text{pwn}}$  increases continuously since the shell expands faster than the ambient ejecta. This expansion phase ends when the PWN collides with the reverse shock of the SNR. After the collision, the pressure inside the nebula  $P_{\text{pwn}}$  is much smaller than the pressure of the material around it  $P_{\text{snr}}(R_{\text{pwn}})$ . The velocity of the PWN decreases greatly, and finally the PWN is compressed. During this process of compression, the magnetic field strength in the nebula increases significantly. Furthermore, the radius of the PWN decrease significantly, and the PWN will expand again when the inner pressure eventually becomes bigger than that of the surrounding ejecta. The nebula experiences a series of contractions and re-expansions until the SNR enters the radiative phase of its evolution. The pulsar moving in the space will leave the PWN during the compression, and it can re-enter the nebula when the nebula expands again. With the parameters in Table.1, the pulsar firstly leaves the nebula at  $\sim 13700 \text{ yr}$ , and re-enters it at  $\sim 19000 \text{ yr}$ .

### 2.3. Application to G12.8-0.0 and discussion

The shell with a diameter of  $\sim 2.5'$ , corresponding to a radius of 1.7 pc for a distance of 4.7 kpc, of the SNR G12.8-0.0 had been revealed with the radio observations with a spectral index of  $\sim -0.48$  (Brogan et al. 2005). Moreover, a pulsar wind nebula with a diameter of  $\sim 80''$  embedded in the SNR was been disclosed in the observations from the X-ray to soft  $\gamma$ -ray bands (Ubertini et al. 2005; Funk et al. 2007; Helfand et al. 2007). An energetic pulsar with a spin-down power bigger than  $10^{37} \text{ erg s}^{-1}$  is argued to exist in the nebula based on the ASCA and Chandra observations (Helfand et al. 2007). Recently, the energetic pulsar PSR J1813-1749 associated the PWN was discovered in the long, continuous *XMM-Newton* X-ray timing observation, and the pulsar has a period of  $\sim 44.7 \text{ ms}$ , a spin-down age of  $3.3 - 7.5 \text{ kyr}$ , and a spin power of  $6.8 \pm 2.7 \times 10^{37} \text{ erg s}^{-1}$  (Gotthelf & Halpern 2009).

The small radius places the SNR G12.8-0.0 amongst the smallest known SNRs, which also suggests a young age for the remnant. In the model, the radius of the SNR is deter-

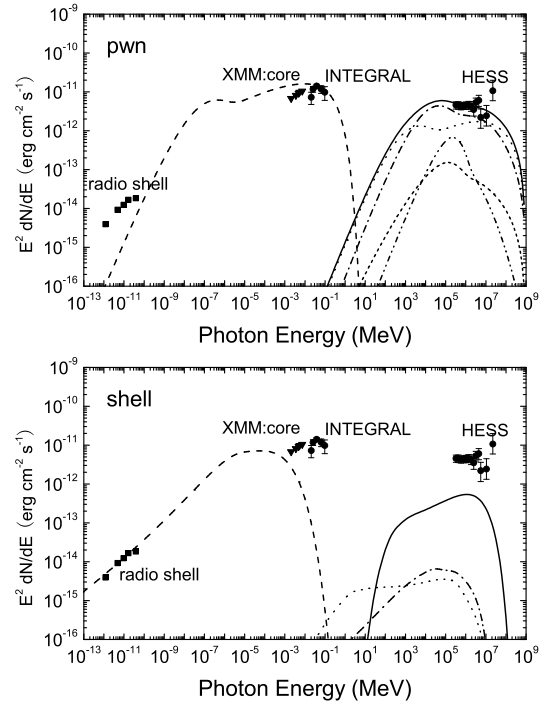


FIG. 4.— Upper panel: the spectral energy distribution for the PWN in G12.8-0.0 at an age of 1200 yr. Synchrotron radiation (dashed line), and IC scattering on the CMB (dotted line), IR (dash-dotted line), star light (dash-dot-dot line) and the synchrotron photons (short dashed line) are shown in the figure. The solid line represents the whole IC scattering on all the soft photons. Lower panel: the spectral energy distribution of the emission from the shell of the SNR G12.8-0.0. Synchrotron radiation (dashed line), bremsstrahlung (dotted line) IC scattering (dash-dotted line) of the accelerated electrons and p-p interactions (solid line) of the accelerated protons are demonstrated in the figure. The radio data are from the VLA, Bonn, Parkes, and Nobeyama observatories (Brogan et al. 2005). The X-ray data are from *XMM-Newton* (Funk et al. 2007) and *INTEGRAL* (Ubertini et al. 2005). The HESS flux points in the VHE  $\gamma$ -ray band are from Aharonian et al. (2006).

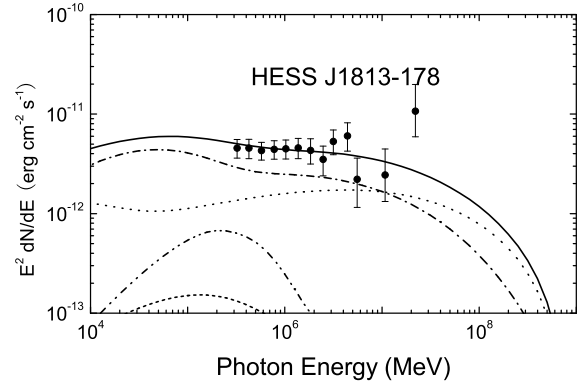


FIG. 5.— A zoomed view of the resulting spectrum and the HESS results in the TeV band. Others are the same as the upper panel in Fig.4.

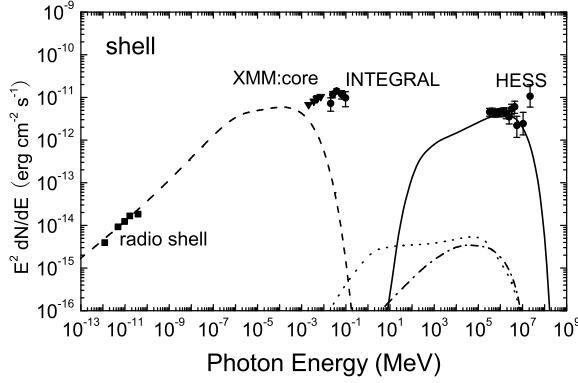


FIG. 6.— the spectral energy distribution of the emission from the shell for  $n_0 = 2.8 \text{ cm}^{-3}$  and  $K_{ep} = 4.5 \times 10^{-4}$ . The others are the same as the lower panel of Fig.4.

mined by the explosion energy, the mass of the ejecta, the ambient density, and the age of the system. We find that, with  $E_{\text{sn}} = 0.4 \times 10^{50} \text{ erg}$ ,  $M_{\text{ej}} = 3M_{\odot}$ , and an ambient ISM density  $n_0 = 1.4 \text{ cm}^{-3}$ , the resulting radius of the SNR shell is  $\sim 1.8 \text{ pc}$  at an age of  $\sim 1200 \text{ yr}$ , which is consistent with the radius of the radio shell. With a larger explosion energy ( $E_{\text{sn}} \geq 10^{50} \text{ erg}$ ) or a smaller ambient density ( $n_0 \leq 0.1 \text{ cm}^{-3}$ ), the age of the system, which is constrained by the radius of the SNR, is much smaller the radius of the radio shell, and the resulting flux of X-ray emission from the PWN is usually much higher than the observed one by *XMM-Newton* (Funk et al. 2007) and *INTEGRAL* (Brogan et al. 2005) since the magnetic field is stronger for a smaller age (see the lower panel of Fig.3). A sub-energetic explosion with  $E_{\text{sn}} \leq 10^{50} \text{ erg}$  and a low ejecta mass  $M_{\text{ej}} = 3M_{\odot}$  was also argued to exist from the multiwavelength study of the newly discovered SNR G310.0-1.6 (Renaud et al. 2009). With  $\tau_{\text{sd}} = 500 \text{ yr}$  and  $\dot{E}_0 = 4.2 \times 10^{38} \text{ erg s}^{-1}$ , the spin-down power is  $3.6 \times 10^{37} \text{ erg s}^{-1}$  at an age of 1200 yr from Eq.14, which is a little smaller than the present observed value, i.e.,  $6.8 \pm 2.7 \times 10^{37} \text{ erg s}^{-1}$  (Gotthelf & Halpern 2009). The radius of the PWN at this age is 0.7 pc, and the ratio  $R_{\text{pwn}}/R_{\text{snr}}$  is  $\sim 0.4$ . The resulting multiband radiation from the PWN in the composite SNR G12.8-0.0 at an age of 1200 yr is shown in the upper panel of Fig.4 with the parameters in Table1. In the figure we also plot the observed data from radio to TeV band for comparison. The data sources are reported in the figure caption. For each panel, the interstellar soft photons scattered in the IC process contain the CMB, IR ( $T_{\text{IR}} = 35 \text{ K}$ ,  $U_{\text{IR}} = 1.0 \text{ eV cm}^{-3}$ ) and star light ( $T_{\text{st}} = 3000 \text{ K}$ ,  $U_{\text{st}} = 1.5 \text{ eV cm}^{-3}$ ). The observed emission detected with *XMM-Newton* and *INTEGRAL* from the X-ray to hard X-ray bands can be explained as the synchrotron radiation from the electrons injected in the PWN, although the resulting flux is a little higher than that observed with *XMM-Newton*. In the VHE  $\gamma$ -ray band, the photons are mainly produced via IC scattering of the electrons in the nebula on the CMB and IR photons from interstellar dust (Fig.5).

The upstream temperature for a SNR varies between  $\sim 10^4 \text{ K}$  for a typical ISM up to  $\sim 10^7 \text{ K}$  if the SNR expands in the hot bubble generated by the progenitor's wind (Chevalier & Liang 1989; Morlino, Amato & Blasi 2009; Berezhko & Völk 2010). We assume the SNR G12.8-0.0 is expanding in the typical ISM with a temperature of

$\sim 10^4 \text{ K}$  to investigate the multiband nonthermal emission from the SNR shell. At an age of 1200 yr, the velocity of the SNR shock is  $\sim 1000 \text{ km s}^{-1}$ , corresponding to a Mach number of  $\sim 86$  for  $T_0 = 10^4 \text{ K}$ . With these parameters,  $R_{\text{tot}}$  and  $R_{\text{sub}}$  are about 8.1 and 3.55, respectively, and the downstream temperature  $T_2$  is  $3.8 \times 10^6 \text{ K}$ . Moreover, the maximum energies of the accelerated protons and electrons are about 60 TeV and 4 TeV, respectively. The energy contained in the protons accelerated by the shock is  $5 \times 10^{48} \text{ erg}$ , and it in the electrons is  $6 \times 10^{45} \text{ erg}$ . Therefore, about 12% of the explosion energy  $E_{\text{sn}}$  has been converted to the kinetic energy of the particles. The amplified magnetic field strength immediately upstream of the subshock is  $62 \mu\text{G}$ , and then the downstream magnetic field strength is  $220 \mu\text{G}$ . With this downstream magnetic field strength and  $K_{ep} = 1.8 \times 10^{-3}$ , the flux points of the radio shell can be reproduced as synchrotron radiation of the electrons accelerated by the SNR forward shock wave; whereas the flux from p-p collisions of the accelerated protons on the ambient matter is significantly smaller than that observed with HESS.

The ISM number density  $n_0$  is an important parameter which can greatly influence the multiband nonthermal emission from the SNR shell. With a larger  $n_0$ , both the density of the accelerated particles and that downstream of the shock increase accordingly. As a result, the flux of the p-p collisions is enhanced with  $\propto n_0^2$ , and then a smaller  $K_{ep}$  is usually needed to reproduce the observed radio fluxes for a denser medium. In order to reproduce the HESS flux in the TeV band via p-p collisions from protons accelerated by the SNR shell, a denser medium with a density of  $2.8 \text{ cm}^{-3}$  must be used in the model (see Fig.6). For  $n_0 = 2.8 \text{ cm}^{-3}$  and the other parameters the same as Fig.4, the multiband nonthermal emission from the PWN is nearly the same as that for  $n_0 = 1.4 \text{ cm}^{-3}$ , whereas the  $\gamma$ -ray flux for the p-p collisions in the SNR shell is comparable to the HESS result; the downstream magnetic field strength is  $271 \mu\text{G}$ , and then a smaller  $K_{ep} = 4.5 \times 10^{-4}$  is needed to reproduced the observed fluxes in the radio band. In this SNR-dominated scenario, the  $\gamma$ -ray photon index of the resulting emission is  $< 2$  up to several tens of GeV, whereas it is  $> 2$  at higher energies (Fig.6). On the other hand, the index in the PWN-dominated case is  $< 2$  from 0.1 GeV to 1 TeV (Fig.4). The resulting TeV  $\gamma$ -ray spectral energy distributions in the two scenarios are all consistent with the HESS flux points, so we cannot determine which case is preferred by comparison with the detected fluxes in the TeV range now. However, the flux in the GeV band in the PWN-dominated case is several times higher than in the SNR-dominated case, so future detections in this band can give constraints on the origin of the  $\gamma$ -rays from HESS J1813-178.

Even if a denser medium with  $n_0 \sim 2.8 \text{ cm}^{-3}$  is used in the model to enhance the p-p collisions in the SNR shell, the IC scattering of the electrons/positrons in the PWN is still prominent enough to contribute significantly to the high-energy  $\gamma$ -ray emission from the composite SNR. In the model, the PWN evolves in the remnant with an age of  $\sim 1200 \text{ yr}$ , and high-energy electrons/positrons are injected continuously into the nebula from the energetic pulsar during the evolution. In fact, if the emission detected with *XMM-Newton* and *INTEGRAL* is the synchrotron radiation from the electrons/positrons injected in the PWN, the detected VHE  $\gamma$ -rays can be easily explained by the IC scattering of these electrons/positrons off the ambient soft photons. Therefore, it is natural to argue that the observed high-energy photons from the X-ray to VHE  $\gamma$ -ray bands originate mainly from the PWN inside the composite remnant although the contribution of the SNR shell to the



$\gamma$ -rays becomes significant for a denser medium with a density of  $2.8 \text{ cm}^{-3}$ .

### 3. SUMMARY AND CONCLUSION

The origin of the VHE  $\gamma$ -rays from HESS J1813-178 is investigated in this paper. Although the source is pointlike in VHE  $\gamma$ -rays, a shell origin of the VHE  $\gamma$ -rays cannot be ruled out because the PSF of the HESS telescope is very close to the size of the SNR's shell (e.g., Albert et al. 2006). A SNR with a diameter of  $2.5'$  was identified in the radio bands to be associated with the VHE  $\gamma$ -ray source. Moreover, X-ray observations showed a PWN powered by an energetic pulsar is embedded in the SNR (Brogan et al. 2005; Ubertini et al. 2005; Funk et al. 2007; Helfand et al. 2007), and the pulsar was recently discovered in a long, continuous *XMM-Newton* X-ray timing observation (Gotthelf & Halpern 2009). We apply a model which can self-consistently calculate the multi-wavelength nonthermal emission both from the SNR shell and from the PWN embedded in the remnant. In the model, electrons/positrons with a spectrum of a relativistic Maxwellian plus a power-law high-energy tail are injected in the nebula during the PWN during its evolution inside the SNR; protons and electrons are accelerated by the SNR shock wave, and the spectrum of the accelerated particles are calculated with a semi-analytical non-linear model. Our results indicate that: with the parameters in Table 1, (1) the observed emission of the shell in the radio bands can be well explained as synchrotron radiation of the electrons accelerated by the SNR shock wave, whereas the flux of p-p collisions of the accelerated protons is significantly smaller than the TeV flux observed with HESS; (2) the observed emission in the X-ray to hard X-ray band detected with *XMM-Newton* and *INTEGRAL*, respectively, can be explained as the synchrotron radiation of the electrons/positrons injected in the PWN; (3) the VHE  $\gamma$ -rays in the TeV band are mainly produced via IC scattering of the electrons/positrons injected in the nebula on the CMB and

interstellar IR photons.

With a sub-energetic explosion ( $E_{\text{sn}} \sim 0.4 \times 10^{50} \text{ erg}$ ), an age of  $\sim 1200 \text{ yr}$ , and an ambient density of  $1.4 \text{ cm}^{-3}$ , the radius of the composite SNR G12.8-0.0,  $1.7 \text{ pc}$ , as well as the multiband observed nonthermal fluxes for the remnant can be reproduced within this model described in this paper. The present value of the SNR shock's velocity is about  $1000 \text{ km s}^{-1}$ , and the VHE  $\gamma$ -rays are predominately produced from the nebula inside the remnant via IC scattering. Of course, p-p interaction from the SNR shell can be enhanced with a denser medium around the remnant (Fig. 6). Even if this condition were satisfied, the  $\gamma$ -rays produced via IC scattering in the PWN remain significant, hence, in this case, both the SNR shell and the PWN would contribute to the production of the observed  $\gamma$ -ray flux. In GeV  $\gamma$ -rays, the spectral property of the resulting emission in this SNR-dominated scenario (Fig. 6) differs significantly from that in the PWN-dominated case (Fig. 4). The VHE  $\gamma$ -rays of HESS J1813-178 detected with HESS can be naturally explained as the IC scattering of the electrons/positrons injected into the PWN although the p-p collisions become important with a denser ambient medium for the remnant. Our study give more insights on the nature of the multiband nonthermal emission of the composite SNR G12.8-0.0, even though some assumptions are made in the model.

### ACKNOWLEDGMENTS

We are very grateful to the anonymous referee for his/her helpful comments to improve the paper. This work is partially supported by the Scientific Research Foundation of Graduate School of Yunnan University, the National Natural Science Foundation of China (NSFC 10778702, 10803005), a 973 Program (2009CB824800), and Yunnan Province under a grant 2009 OC.

### REFERENCES

- Aharonian, F., et al. (HESS Collaboration) 2005a, *Science*, 307, 1938  
 Aharonian, F., et al. (HESS Collaboration) 2005b, *A&A*, 437, L7  
 Aharonian, F., et al. (HESS Collaboration) 2006, *ApJ*, 636, 777  
 Aharonian, F. et al. (HESS Collaboration), 2007, *A&A*, 464, 235  
 Albert, J. et al. 2006, *ApJ*, 637, L41  
 Amato, E., Blasi, P., & Gabici, S., 2008, *MNRAS*, 385, 1946  
 Atoyan, A. M., & Aharonian, F. A. 1996, *MNRAS*, 278, 525  
 Berezhko, E. G., Ksenofontov, L. T. & Völk, H. J. 2002, *A&A*, 395, 943  
 Berezhko, E. G., & Völk, H. J., 2006, *A&A*, 419, L27  
 Berezhko, E.G. & Völk, H.J. 2006, *A&A*, 451, 981  
 Berezhko, E.G. & Völk, H.J. 2010, *A&A*, 511, 34  
 Blasi P., 2002, *Astropart. Phys.*, 16, 429  
 Blasi, P., 2010, *MNRAS*, 402, 2807  
 Blasi P., Gabici S., & Vannoni G., 2005, *MNRAS*, 361, 907  
 Brogan, C. L. 2005, *ApJ*, 629, L105  
 Caprioli, D., Blasi, P., Amato, E., & Vietri, M. 2009, *MNRAS*, 395, 895  
 Caprioli, D., Amato, E., Blasi, P. 2010, *Astropart. Phys.*, 33, 160  
 Caprioli, D., Amato, E., Blasi, P., 2010, *Astropart. Phys.*, 33, 307  
 Chevalier, R. A., & Liang, E. P. *ApJ*, 344, 332  
 Ellison D. C., Berezhko E. G., Baring M. G., 2000, *ApJ*, 540, 292  
 Fang, J., & Zhang, L., 2008, *MNRAS*, 384, 1119  
 Fang, J., Zhang, L., Zhang J. F., Tang, Y. Y. & Yu, H. 2009, *MNRAS*, 392, 925  
 Fang, J., & Zhang, L. 2010, *A&A*, in press (arXiv:1003.1656)  
 Funk, S., et al. 2007, *A&A*, 470, 249  
 Gaensler, B. M., & Slane, P. O. 2006, *ARA&A*, 44, 17  
 Gelfand, J. D., Gaensler, B. M., Slane, P. O., Patnaude, D. J., Hughes, J. P., & Camilo, F. 2007, *ApJ*, 663, 468  
 Gelfand, J. D., Slane, P. O., & Zhang, W. 2009, *ApJ*, 703, 2051  
 Gotthelf, E. V., & Halpern, J. P. 2009, *ApJ*, 700, L158  
 Helfand, D. J., Gotthelf, E. V., Halpern, J. P., Camilo, F., Semler, D. R., Becker, R. H., & White, R. L. 2007, *ApJ*, 665, 1297  
 Kamae T., Karlsson N., Mizuno T., Abe T., Koi T., 2006, *ApJ*, 647, 692  
 Malkov M. A., Drury, L. O'C. 2001, *Rep. Prog. Phys.*, 64, 429  
 Morlino, G., Amato, E., & Blasi, P. 2009, *MNRAS*, 392, 240  
 Morlino, G., Amato, E., Blasi, P., & Caprioli, D. 2009, arXiv:0912.2972  
 Renaud, M., Marandon, V., Gotthelf, E. V., Rodriguez, J., Terrier, R., Mattana, F., Lebrun, F., Tomsick, J. A., Manchester, R. N. 2010, *ApJ*, 716, 663  
 Slane, P. 2008, *AIPC*, 1085, 120  
 Slane, P., Helfand, D. J., Reynolds, S. P., Gaensler, B.M., Lemiére, A., & Wang, Z. 2008, *ApJ*, 676, L33  
 Slane, P., Castro, D., Funk, S., Uchiyama, Y., Lemiére, A., Gelfand, J. D., & Lemoine-Goumard, M. 2010, (arXiv:1004.2936)  
 Spitkovsky, A. 2008, *ApJ*, 682, L5  
 Truelove, J. K., & McKee, C. F. 1999, *ApJS*, 120, 299  
 Ubertini, P. et al. 2005, *ApJ*, 629, L109  
 Venter, C., & de Jager, O. C. 2006, in *Proc. 363rd WE-Heraeus Seminar, Neutron Stars and Pulsars*, ed. W. Becker & H. H. Huang (MPE Report 291; Garching: MPE), 40  
 Volpi, D., Del Zanna, L., Amato, E. & Bucciantini, N. 2008, *A&A*, 485, 337  
 Zhang, L., Chen, S. B., & Fang, J. 2008, *ApJ*, 676, 1216  
 Zirakashvili, V. N., & Aharonian, F., 2007, *A&A*, 465, 695